ADVANCED FUNCTIONAL MATERIALS
www.afm-journal.de

Materials Views
www.MaterialsViews.com

Nanostructured Alkaline-Cation-Containing δ-MnO_2 for Photocatalytic Water Oxidation

*Venkata Bharat Ram Boppana, Seif Yusuf, Gregory S. Hutchings, and Feng Jiao**

Oxygen evolution from water is one of the key reactions for solar fuel production. Here, two nanostructured K-containing δ-MnO_2 are synthesized: K-δ-MnO_2 nanosheets and K-δ-MnO_2 nanoparticles, both of which exhibit high catalytic activity in visible-light-driven water oxidation. The role of alkaline cations in oxygen evolution is first explored by replacing the K^+ ions in the δ-MnO_2 structure with H^+ ions through proton ion exchange. H-δ-MnO_2 catalysts with a similar morphology and crystal structure exhibit activities per surface site approximately one order of magnitude lower than that of K-δ-MnO_2, although both nanostructured H-δ-MnO_2 catalysts have much larger Brunauer–Emmett–Teller (BET) surface areas. Such a low turnover frequency (TOF) per surface Mn atom might be due to the fact that the $Ru^{2+}(bpy)_3$ sensitizer is too large to access the additional surface area created during proton exchange. Also, a prepared Na-containing δ-MnO_2 material with an identical crystal structure exhibits a TOF similar to that of the K-containing δ-MnO_2, suggesting that the alkaline cations are not directly involved in catalytic water oxidation, but instead stabilize the layered structure of the δ-MnO_2.

1. Introduction

Efficient harvesting of solar energy is an important technological challenge considering that the energy of sunlight that strikes the earth's surface in an hour is sufficient to meet our energy demands for a year.[1–4] Moreover, an economic and mobile energy-storage medium that does not affect the current energy infrastructure is necessary to offset the diffuse and intermittent nature of sunlight. These dual issues could be resolved by generating transportable solar fuels (like hydrogen or methanol) from abundant sources (e.g., H_2O and CO_2) utilizing sunlight as the primary energy source.[1–3] Multiple approaches, including photo-electrochemical and photocatalytic methods, have been proposed and investigated in recent years.[5–14] Irrespective of the approach that is pursued, oxygen evolution from water is the critical reaction, because water is the only cheap, clean, and abundant source that is capable of completing the redox cycle for producing either hydrogen (from H_2O) or carbonaceous fuels (from CO_2) on a terawatt scale.[1,15–23] Thus, an effective catalyst for oxygen evolution via water oxidation is the key component for accomplishing the challenge of efficient solar-energy harvesting.

A further challenge is in combining both absorption of light along with catalyzing the four-electron process of water oxidation. Nature achieves this by using chlorophyll complexes for efficient charge separation after light absorption and a different $CaMn_4O_4$ system for catalyzing the oxidation of H_2O to O_2.[24] Earlier efforts have focused on iridium oxide particles; for example, Mallouk and co-workers achieved a turnover frequency (TOF) of 40 s^{-1} with this material in a $Ru^{2+}(bpy)_3$ photocatalytic system.[25] While this is promising, the cost of iridium is prohibitively expensive for widespread usage. Inspired by nature's calcium manganese oxide catalyst system, recent efforts have therefore focused on the development of less-expensive transition metal oxides.[26–39] For example, we recently reported the utilization of manganese and cobalt oxides nanoclusters inside mesoporous supports for artificial water-oxidation applications in visible light.[40,41] The higher activity for these nanocatalysts compared with their micrometer-sized counterparts was attributed in part to the high surface areas afforded by the small nanoclusters inside the pores of the silica supports. We then proceeded to investigate systematically the influence of the crystal structure of manganese oxide systems on the water-oxidation activity.[42] All of the samples exhibited high TOFs and we concluded that the morphology and crystal structure have a negligible effect on the water-oxidation activity for MnO_2 catalysts, while larger surface areas significantly enhanced their activity in line with our earlier studies with silica supports. We also noted in that work that the presence of potassium in α-MnO_2 nanotubes improves the activity and this report extends on this hypothesis by carefully elucidating the effect of potassium on the water-oxidation activity by discounting other variables like surface area, crystal structure, and morphology.

Manganese (IV) oxide exists in multiple polymorphs: α, β, γ, and δ-MnO_2. All of these four crystal structures are made of $[MnO_6]$ octahedral units: α, β, and γ-MnO_2 are respectively based on 2×2, 1×1, 1×2 Mn octahedral tunnels whereas δ-MnO_2 has a layered structure (see Supporting Information, Figure S1).[43] Of these four major polymorphs of MnO_2,

Dr. V. B. R. Boppana, S. Yusuf, G. S. Hutchings, Prof. F. Jiao
Department of Chemical and Biomolecular Engineering
University of Delaware
Newark, DE, 19716, USA
E-mail: jiao@udel.edu

DOI: 10.1002/adfm.201202141

α-MnO_2 and δ-MnO_2 have channels big enough to uptake guest cations like K^+, which has been noted in studies by Komaba and co-workers and our earlier work.[42,44] These two polymorphs therefore form the basis of this study, especially δ-MnO_2, since its layers can incorporate a higher fraction of K^+. Due to this property, this material is known to favor the diffusion of Li^+ and has therefore already been investigated for lithium battery applications.[43] On the other hand, β-MnO_2 has the smallest channels formed by 1×1 edge-shared Mn octahedral structures, and shows no capability in taking up any guest cations. These variations in the uptake of cations (in our case, K^+ and Na^+) prompted us to analyze systematically the effect of alkaline cations on the water-oxidation activity with manganese oxide systems, as this has not been explored so far. This work demonstrates that δ-MnO_2 materials containing alkaline cations are effective water-oxidation catalysts.

2. Results and Discussion

Several techniques detailed in literature were employed to synthesize nanostructured K-δ-MnO_2. K-δ-MnO_2 nanosheets were synthesized according to the procedure reported by Li.[45] To clarify the effect of morphology, K-containing δ-MnO_2 nanoparticles were also synthesized through a solid-state reaction of thermal decomposition of $KMnO_4$ at 300 °C.[46] A K-δ-MnO_2 material with a much larger particle size and lower surface area was synthesized by the same technique at a higher calcination temperature (800 °C) in order to facilitate the investigation of surface effects in photocatalytic water oxidation. Also, proton ion exchange was performed for both K-δ-MnO_2 nanosheets and nanoparticles to replace K^+ with H^+ in the δ-MnO_2 structures. All of the synthesis conditions are detailed in the experimental section.

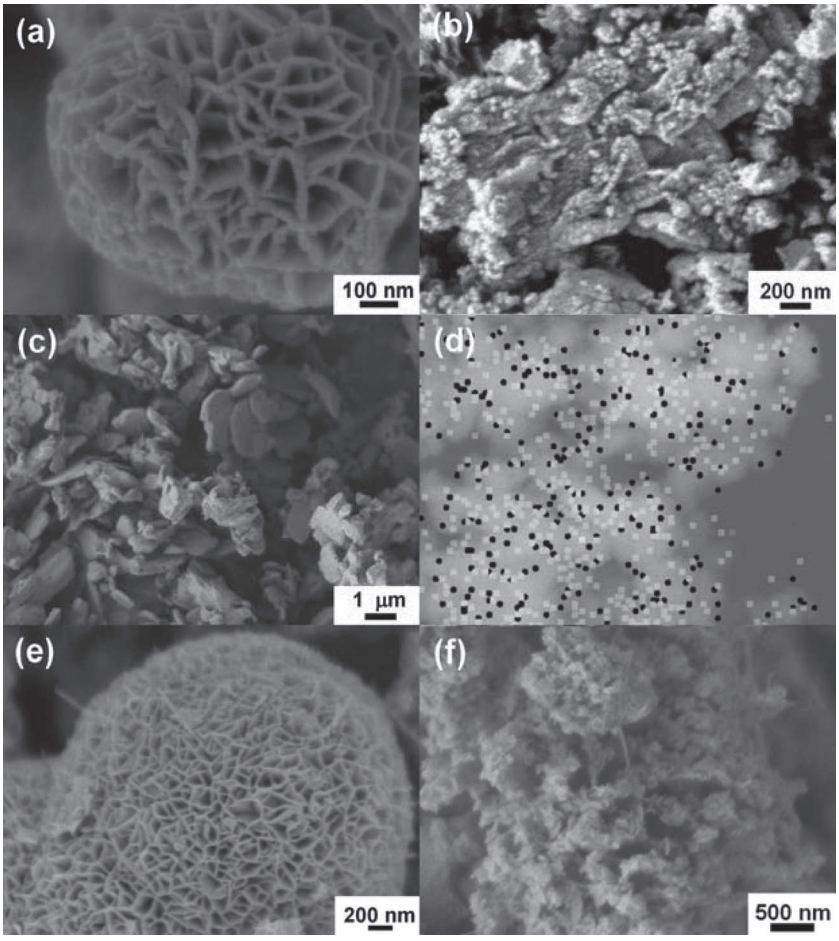

Figure 1. a–d) SEM images for as-prepared nanostructured δ-MnO_2 materials: K-δ-MnO_2 nanosheets (a), K-δ-MnO_2 nanoparticles (b), K-δ-MnO_2 micrometer-sized particles (c); elemental mapping of K-δ-MnO_2 nanosheets (dark dots for K and light-gray dots for Mn) (d). e,f) SEM images for nanostructured δ-MnO_2 materials after proton ion exchange: H-δ-MnO_2 nanosheets (e) and H-δ-MnO_2 nanoparticles (f).

We first examined the morphologies of K-δ-MnO_2 samples using scanning electron microscopy (SEM). The SEM image (**Figure 1**a) clearly shows that the morphology of K-δ-MnO_2 prepared via hydrothermal reaction is of spheres composed of nanosheets. Each sphere is about 1 μm in diameter and its nanosheets are around 10–20 nm thick. In the cases of K-δ-MnO_2 prepared through thermal decomposition reaction at 300 °C and 800 °C, no such morphology is observed (Figure 1b,c). The 300 °C sample contains small particles with a dimension of 10–200 nm, while the 800 °C sample has an average particle size of 0.5–1 μm. Energy-dispersive X-ray (EDX) spectroscopy measurements show that the K-δ-MnO_2 nanosheets and the K-δ-MnO_2 samples synthesized by the solid-state reaction have significant potassium contents with a K/Mn ratio between 0.30 to 0.34 (see supporting information). SEM elemental mapping was then employed to verify the uniform distribution of potassium. The results presented in Figure 1d show that K is distributed uniformly with Mn in all of the δ-MnO_2 particles (see Supporting Information for a color-coded version).

These results are in contrast to the potassium contents observed after proton ion exchange. Reaction of the K-δ-MnO_2 samples with 0.7 M of HNO_3 reduces the K/Mn ratio from ≈0.32 to 0.02. This suggests that K^+ cations in the layered δ-MnO_2 structure are leached away and replaced with H^+ under aggressive acid treatment. The H-δ-MnO_2 nanosheets prepared through the hydrothermal reaction maintained their morphology after acid treatment (Figure 1e), while the K-δ-MnO_2 nanoparticles prepared at 300 °C became rougher on the surface and some nanorod-like particles were observed after proton exchange (Figure 1f).

We performed high-resolution transmission electron microscopy (HR-TEM) to further explore the structural details of the K-δ-MnO_2 samples. The HR-TEM images in **Figure 2** show that both as-prepared K-δ-MnO_2 samples were composed of MnO_2

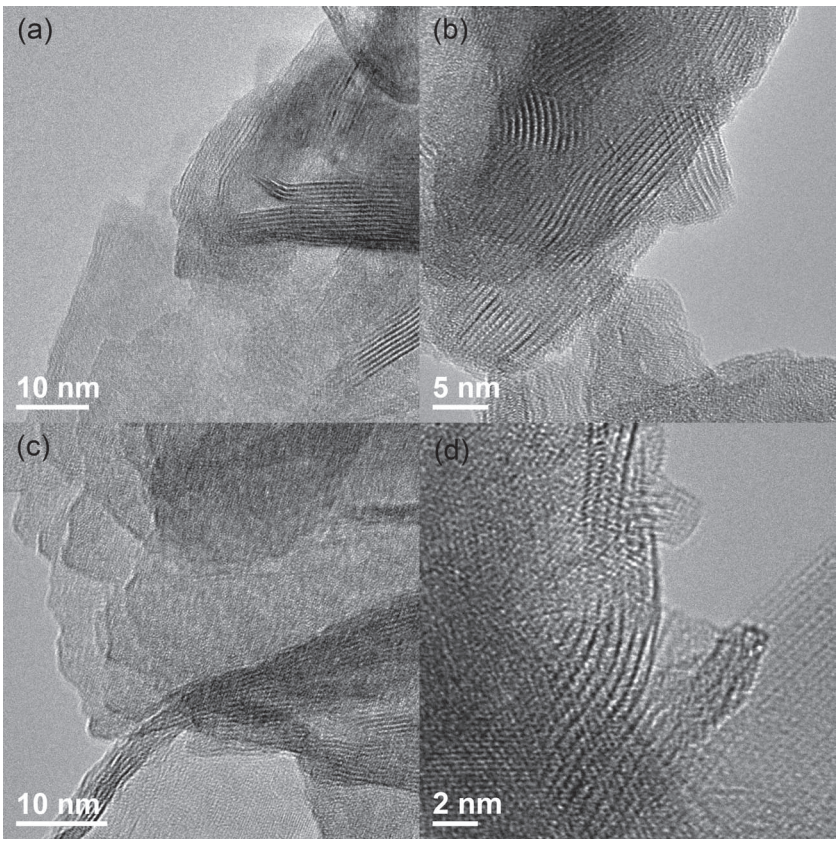

Figure 2. HR-TEM images for as-prepared K-δ-MnO_2 nanosheets (a), K-δ-MnO_2 nanoparticles (b), H-δ-MnO_2 nanosheets (c) and H-δ-MnO_2 nanoparticles (d).

nanosheets with the same interlayer distance (≈0.66 nm), indicating that both the materials have a similar crystal structure. This was further confirmed by powder X-ray diffraction (PXRD) analysis. The PXRD patterns (**Figure 3**) confirm the formation of the desired δ-MnO_2 polymorph as all of the observed reflections were indexed to its well-known layered structure. The representative (00*c*) peaks are at ≈12.4°, 24.8° and 36.3° (2θ).

The HR-TEM images for the samples after proton exchange (Figures 2c,d) clearly show that the δ-MnO_2 layered features in both materials were maintained, although in the case of H-δ-MnO_2 nanaoparticles, some nanorod like H-δ-MnO_2 particles are also observed which is consistent with the SEM results. The preservation of the δ-MnO_2 crystal structure was further investigated by the PXRD analysis, shown in Figure 3. Note that the diffraction peaks from the (00*c*) planes are still present. This indicates that the δ-MnO_2 structure was intact, although the relative intensities are slightly different. This could be due to partial destabilization of the layered structure from the leaching of K^+ cations. This destabilization also causes a significant increase in the surface area of the δ-MnO_2 materials after proton exchange. For example, the surface area of the nanosheets increases from 35.7 m^2 g^{-1} to 151 m^2 g^{-1} after the potassium is leached away.

The diffraction peaks for the micrometer-sized K-δ-MnO_2 particles synthesized at 800 °C are much narrower and sharper than the other two nanostructured samples, which is due to its highly crystalline nature. A small peak shift to high angle was also observed, indicating the shrinkage of the interlayer distance in the micrometer-sized particles. The crystallite size estimated from the (001) peak using the Scherrer formula is 45.9 nm, which is significantly larger than the size of the nanoparticles (14.8 nm) and in good agreement with the SEM results (Figure 1). This size difference also results in a 3-fold decrease in surface area, from 24.4 m^2 g^{-1} (300 °C) to 8.1 m^2 g^{-1} (800 °C).

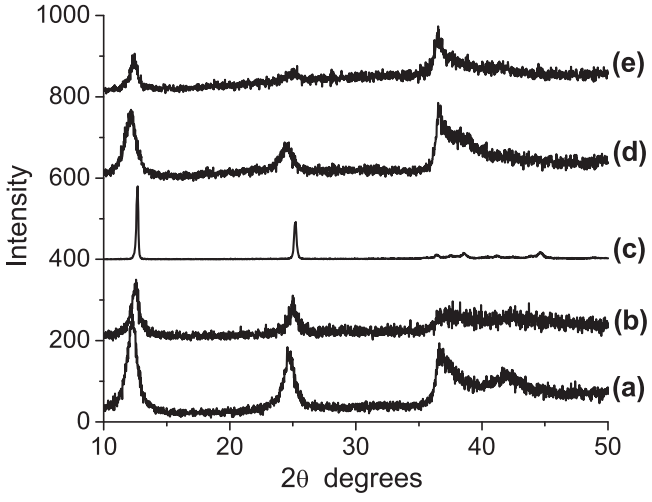

Figure 3. PXRD patterns for: K-δ-MnO_2 nanosheets (a), K-δ-MnO_2 nanoparticles (b), K-δ-MnO_2 micrometer-sized particles (c), H-δ-MnO_2 nanosheets (d), and H-δ-MnO_2 nanoparticles (e).

The oxidation states of the manganese ions in all of the δ-MnO_2 materials were examined by the X-ray absorption near-edge structure (XANES) technique. The results are shown in **Figure 4**a,b. Two standard manganese oxides (MnO_2– Mn^{4+} and Mn_2O_3– Mn^{3+}) are also presented for comparison. It is evident that the K-edges of Mn for all the K-containing δ-MnO_2 samples overlap the K-edge of bulk MnO_2, indicating that the K-δ-MnO_2 samples have an average Mn oxidation state of 4+. Although it is expected that the insertion of alkaline cations into MnO_2 channels decreases the oxidation state of Mn due to the charge balance, the phenomenon observed in the K-containing δ-MnO_2 samples could be explained as the formation of oxygen-rich manganese oxide phases, which has also been reported in previous literature.[46–48] For the proton version of nanostructured δ-MnO_2, the XANES curves (Figure 4b) closely match the data for their potassium-version counterparts, suggesting that the proton-exchange process did not affect the oxidation state of Mn in both nanostructures.

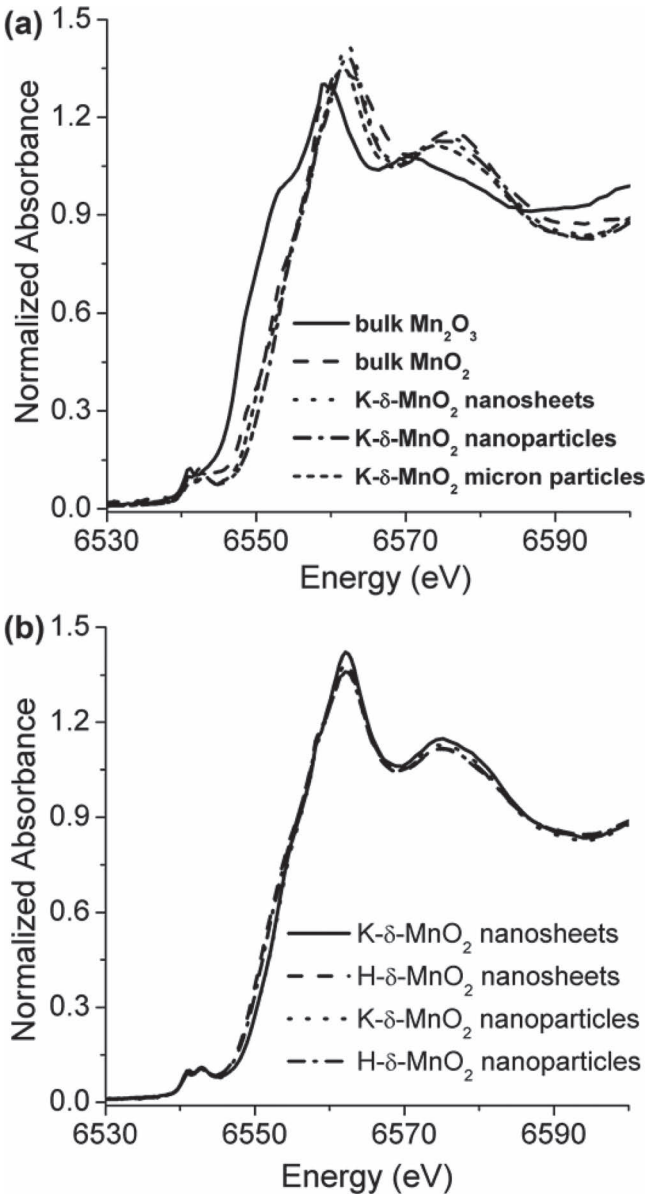

Figure 4. XANES data for: nanostructured and micrometer-sized K-δ-MnO_2 (a) and nanostructured H-δ-MnO_2 (b).

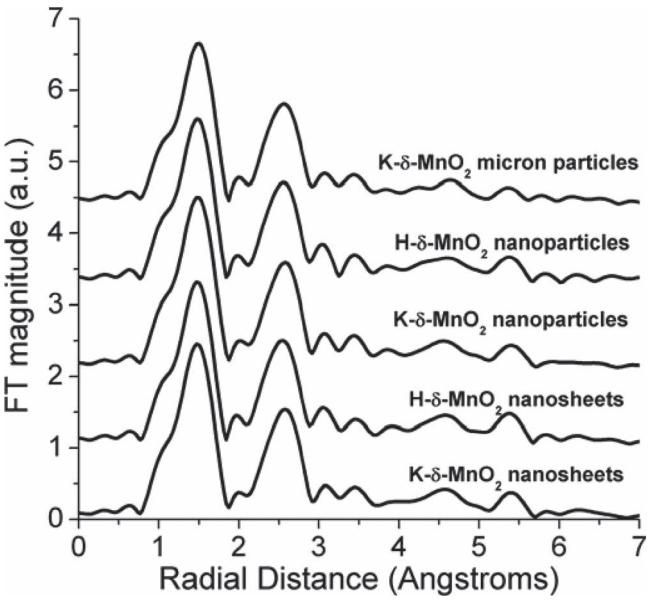

Figure 5. EXAFS data for all the δ-MnO_2 materials; the curves are shifted along the *y*-axis for display purposes.

The crystal structures of all of the δ-MnO_2 samples were also investigated by the extended X-ray-absorption fine-structure (EXAFS) technique. The *R*-space results presented in **Figure 5** show that all of the peaks match perfectly, even at long radial distances, confirming that all of the δ-MnO_2 samples have the same crystal structure, regardless of their morphologies, even after replacing all the potassium ions with protons. This is in good agreement with the PXRD analysis (Figure 3). The similarity in the morphology, crystal structure, and oxidation state of Mn for K-δ-MnO_2 and H-δ-MnO_2 described above using multiple techniques is essential in exploring the role of alkaline cations in catalytic water oxidation.

For photocatalytic water-oxidation experiments, a $Ru^{2+}(bpy)_3$-$S_2O_8^{2-}$ sacrificial water-oxidation system was utilized in this work. To restate briefly, the $Ru^{2+}(bpy)_3$ sensitizer acts as the visible-light absorber, and the lamp source used was a 300 W Xe lamp (Thermo–Oriel) fitted with a 400 nm cut-off filter. Electron-hole pairs were then generated and the sensitizer transferred the photogenerated electrons to sodium persulfate, a sacrificial electron acceptor. The photogenerated holes were passed to the water-oxidation catalyst, MnO_2. During this whole process, $S_2O_8^{2-}$ is reduced to SO_4^{2-} and $Ru^{2+}(bpy)_3$ is oxidized to $Ru^{3+}(bpy)_3$. This cycle was repeated 2 times to produce one oxygen molecule, as one photon produces two $Ru^{3+}(bpy)_3$. The O_2 molecules thus generated after 1 h of illumination were quantitatively analyzed by gas chromatography, using a pulsed discharge helium ionization detector (PDHID) detector capable of detecting ppm levels of O_2. No increase in oxygen levels were detected when no light source was utilized or when the lamp was switched on but when no catalyst was employed. Similarly, no oxygen concentration increase was detected when no sensitizer $Ru^{2+}(bpy)_3$ was used. These control experiments clearly indicate that the observed increase in oxygen concentration is photocatalytic in nature under the experimental conditions.

The photocatalytic water-oxidation activities of the catalysts are shown in **Table 1**. In order to investigate the effect of potassium on the activity of manganese oxides in oxygen evolution, we carefully analyzed the K/Mn ratios by inductively coupled plasma optical-emission spectrometry (ICP-OES) and EDX measurements, which confirmed the K contents in all the catalysts (Table 1). All of the δ-MnO_2 catalysts exhibited a similar TOF of 0.8–1.6 $\times$ 10^{-5} s^{-1} per Mn. After normalizing the TOFs by surface area, the K-containing manganese oxides exhibit TOFs of 5–18 $\times$ 10^{-4} s^{-1} per surface Mn atom, which is about one order higher than their proton-containing counterparts. It is interesting to note that many previously reported manganese oxide water-oxidation catalysts have a very similar TOF per surface Mn atom, such as 1 $\times$ 10^{-3} s^{-1} for λ-MnO_2 (LT), 8 $\times$ 10^{-4} s^{-1}

Table 1. Oxygen production TOFs and BET surface areas of various δ-MnO_2 materials.

δ-MnO_2 Catalyst	TOF [s^{-1} per Mn atom]	BET surface area [$m^2\ g^{-1}$]	TOF [s^{-1} per surface Mn atom]	Alkaline cation to Mn atomic ratio
K-δ-MnO_2 nanosheets	1.47×10^{-5}	35.7	5.20×10^{-4}	0.30
K-δ-MnO_2 nanoparticles	1.56×10^{-5}	24.4	8.04×10^{-4}	0.32
K-δ-MnO_2 micrometer-sized particles	1.17×10^{-5}	8	1.84×10^{-3}	0.34
H-δ-MnO_2 nanosheets	1.00×10^{-5}	151	8.34×10^{-5}	0.02
H-δ-MnO_2 nanoparticles	8.45×10^{-6}	121.6	8.74×10^{-5}	0.02
Na-δ-MnO_2 nanoparticles	9.40×10^{-6}	6	1.97×10^{-3}	0.31

for Mn oxides supported in mesoporous silica, and 7×10^{-4} s^{-1} for a $CaMn_2O_4$ catalyst.[31,32,41]

Compared with proton-containing δ-MnO_2, the K-containing catalysts exhibit higher TOFs per surface Mn atom, although both the nanostructured H-containing δ-MnO_2 samples have much larger surface areas than their potassium versions. The structural analysis, including PXRD, SEM, TEM, XANES and EXAFS, has demonstrated that the crystal structure was maintained throughout the proton-exchange process, while the HR-TEM data (Figure 2) suggest that the layered structure of the H-δ-MnO_2 samples became less ordered compared with that of K-δ-MnO_2. This might be due to the exfoliation of the MnO_2 layers during the proton exchange, leading to ultrahigh surface areas. Although we should expect a higher oxygen-evolution activity from catalysts with a larger surface area, it is clearly not the case in the present study. One possible explanation is that the surface area gained upon the removal of potassium cations can be accessed by only nitrogen molecules in the gas-absorption experiment, but not by a $Ru^{2+}(bpy)_3$ sensitizer (a much larger molecule than N_2) in photocatalytic oxygen evolution. Without a $Ru^{2+}(bpy)_3$ sensitizer available on the catalyst surface, the catalytic sites (surface Mn) lose the capability of catalyzing oxygen evolution from water under visible light. The origin of the low activity of the H-δ-MnO_2 samples could further be explored in an electrocatalytic water-splitting setup, in which no sensitizer is involved. The experiment is still ongoing and will be reported separately. The results in Table 1 are in good agreement with our earlier work as the same set of alkali-metal-containing catalysts show similar TOFs, independent of the catalyst's morphology.[42]

Further studies have been done to clarify the role of potassium in the photocatalytic oxygen-evolution reaction. We synthesized Na-containing δ-MnO_2 nanosheets through a solution-chemistry approach.[47] The SEM image (**Figure 6**a) shows that as-prepared Na-containing δ-MnO_2 had a nanosheet morphology, similar to the K-containing δ-MnO_2 sample. The nanosheets with an average particle size of 200–300 nm aggregated into large secondary particles (a few micrometers) with a poorly defined shape, while the K-δ-MnO_2 nanosheets formed uniform and spherical secondary particles (Figure 1a). This formation of agglomerates could be the reason for the low surface area of 6 $m^2\ g^{-1}$ associated with the Na-δ-MnO_2 material. The HR-TEM image (Figure 6b) confirmed the layered crystal structure of the Na-δ-MnO_2 sample, in good agreement with the PXRD result (Figure 6c). We investigated the oxygen-evolution

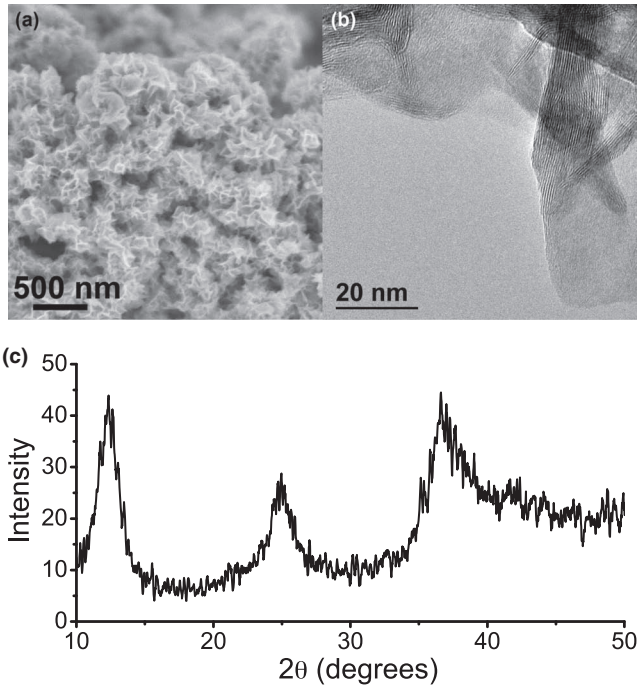

Figure 6. a–c) SEM image (a), HR-TEM image (b), and PXRD pattern (c) for Na-δ-MnO_2 nanosheets.

activity of this Na-δ-MnO_2 sample under identical conditions for K-containing samples. The oxygen evolution results (Table 1) clearly demonstrate that the Na-δ-MnO_2 catalyst exhibits a similar TOF per surface Mn atom compared with the potassium-version of δ-MnO_2, indicating that alkaline ions in both the Na-δ-MnO_2 and K-δ-MnO_2 samples may not directly be involved in photocatalytic oxygen evolution, but instead stabilize the layered structure of δ-MnO_2. Such a finding is also consistent with our previous α-MnO_2 nanotube study, in which we discovered that the catalyst exhibited a similar TOF per Mn atom after aggressive acid treatment.[42]

As a critical characteristic, we proceeded to explore the stability of the nanostructured alkaline-cation-containing δ-MnO_2 nanosheet catalyst. We recovered the catalyst after 1 h of photocatalytic oxygen evolution and re-examined it by SEM and X-ray absorption spectroscopy (XAS). The SEM images for the nanostructured K-δ-MnO_2 clearly show the morphology of the catalysts was maintained, while the EDX results indicate

Table 2. Oxygen-production TOFs and BET surface areas of various δ-MnO_2 materials.

δ-MnO_2 Nanosheet Catalyst	TOF [s^{-1} per Mn atom]
Fresh Catalyst	1.47×10^{-5}
Spent Catalyst–Run 1	1.63×10^{-5}
Spent Catalyst–Run 2	1.49×10^{-5}

a partial potassium-content loss after photolysis (see Supporting Information). Such a loss might be due to the proton exchange during the water-oxidation reaction. We repeated the same water-oxidation experiment as detailed above with the recovered catalyst twice and a similar TOF was observed (see **Table 2**), which suggests that the potassium loss doesn't affect the TOF of the K-δ-MnO_2 catalysts. The XANES and EXAFS data for the K-δ-MnO_2 nanosheets are shown in **Figure 7**. After photocatalysis, a small shift of the Mn K-edge to low energy was observed, which indicates a slight reduction of the Mn oxidation state during the photocatalytic oxygen evolution. The EXAFS data for both before and after photocatalysis show almost identical patterns, confirming the material's structural robustness during oxygen evolution, although, at long radial distances, a slight reduction in the peak intensities for the catalyst after photocatalysis was observed; this may suggest a decrease of long-range atomic ordering. Overall, the K-δ-MnO_2 catalysts exhibit good structural stability and catalytic reproducibility.

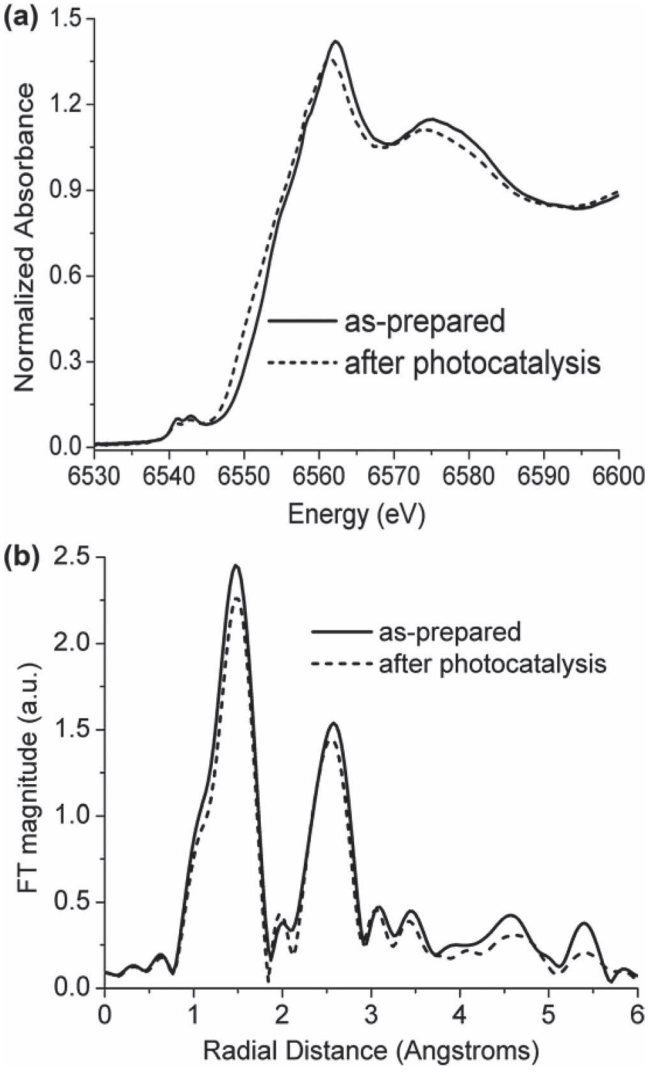

Figure 7. XANES (a) and EXAFS (b) results for the K-δ-MnO_2nanosheets before and after photocatalytic water oxidation.

3. Conclusions

K-containing δ-MnO_2 nanosheets and nanoparticles have been synthesized through hydrothermal and solid-state reactions. Their catalytic properties in water-oxidation reactions driven by visible light have been studied for the first time. The role of alkaline cations in oxygen evolution has been explored through systematic comparison between K-containing δ-MnO_2 and proton-containing δ-MnO_2 with an identical morphology and crystal structure. The two nanostructured K-δ-MnO_2 catalysts exhibited approximately one order of magnitude higher activities per surface site compared with their proton-containing counterparts, although both nanostructured H-δ-MnO_2 catalysts had much larger surface areas. Such a phenomenon might be because the higher surface areas of the nanostructured H-δ-MnO_2 catalysts cannot be accessed by the $Ru^{2+}(bpy)_3$ sensitizer. Also, a sodium-containing δ-MnO_2 with an identical crystal structure was synthesized and it exhibited a similar TOF to the K-δ-MnO_2, suggesting that the alkaline cations are not directly involved into the catalytic water oxidation, but instead stabilize the MnO_2 layers.

4. Experimental Section

Synthesis of K-δ-MnO_2 Nanosheets: This procedure is modified based on a reported approach.[45] In a typical synthesis of K-δ-MnO_2 nanosheets (with K), 0.948 g of $KMnO_4$ was dissolved in water, followed by the addition of 0.169 g of $MnSO_4$ under stirring. The mixture was transferred and sealed in a hydrothermal bomb with a polytetrafluoroethylene (PTFE) liner, followed by thermal treatment in an oven at 160 °C for 12 h. After cooling to room temperature, the resulting mixture was filtered, washed with water, and dried at 60 °C.

Synthesis of K-δ-MnO_2 Nanoparticles: 1 g of $KMnO_4$ was calcined at 300 °C under air for 3 h to form the corresponding K-δ-MnO_2 phases. The resulting materials were dispersed in 200 mL of deionized (DI) water and sonicated for 0.5 h, followed by filtering and several washes with water. The final samples were dried under air at 60 °C. Following a similar procedure, $KMnO_4$ was calcined at 800 °C to obtain micrometer-sized K-δ-MnO_2 particles.[46]

Synthesis of Na-δ-MnO_2 Nanosheets: In a typical synthesis of Na-δ-MnO_2 nanosheets (with Na), 100 mL of $Mn(NO_3)_2$ aqueous solution (containing 3 mmol of Mn) was slowly added into a mixture of 180 mL of NaOH aqueous solution (containing 6.88 g of NaOH) and 20 mL of 30% H_2O_2 under stirring. After stirring at room temperature for 1 h, the resulting precipitate was centrifuged and washed with water, then dried at 60 °C.[47]

Nanostructured Na-δ-MnO_2 by Proton Ion Exchange: 1 g of as-synthesized K-δ-MnO_2 (nanosheets and nanoparticles) was dispersed in 100 mL of 0.7 M HNO_3 aqueous solution. The mixture was heated to 60 °C for 90 min before cooling to room temperature. The mixture was filtered, washed with water, and dried at 60 °C.

Structural Characterization: Scanning electron microscope (SEM) images were recorded on a JEOL JSM 7400F microscope with a field-emission gun capable of 1.5 nm resolution. The imaging using the SEM and elemental analysis with mapping using energy dispersive X-ray (EDX) analysis were done at voltages of 3 kV and 15 kV, respectively. Transmission electron microscope (TEM) images were recorded using a JEM-2010F FasTEM field-emission transmission electron microscope. Powder X-ray diffraction (PXRD) results were collected using a Philips X'pert diffractometer, using a Cu K_α source, a scan rate of 2 s per step, and a step size of $2\theta = 0.02°$. Adsorption isotherms were collected on a Micromeritics ASAP 2010 at 77 K using N_2 as the adsorbent gas. The surface areas were evaluated using Brunauer–Emmett–Teller (BET) theory on the P/P_0 region of 0.05 to 0.4. All of the samples were degassed at 423 K under vacuum before the measurements. X-ray absorption experiments were performed at beamline X10c at the National Synchrotron Light Source (NSLS), Brookhaven National Laboratory (BNL), through a user proposal (PASS form number 20026). The XAS data were processed using the Athena free software.

Photocatalytic Oxygen Evolution from Water: Photochemical water-oxidation experiments were conducted in a 100 mL reactor containing 40 mL of an aqueous buffer (Na_2SiF_6-$NaHCO_3$, 0.022–0.028 M) (with pH held at 5.8), 390 mg of Na_2SO_4, 130 mg of $Na_2S_2O_8$, 45 mg of $[Ru(bpy)_3]Cl_2{\cdot}6H_2O$, and 100 mg of the Mn oxide catalyst. The reactor was irradiated using a 300 W Xe research lamp (UV fused silica, 1.3 inch collimated, F/1, 1.5 inch) with a 400 nm cut-off filter. The resulting O_2 molecules in the head space, collected after 1 h of illumination, were quantitatively analyzed using a Shimadzu gas-chromatography system (Shimadzu 2014). All of the experiments were conducted at room temperature (≈25 °C). A base-line was recorded for each test before exposure to the Xe lamp.

Supporting Information

Supporting Information is available from the Wiley Online Library or from the author.

Acknowledgements

V.B.R.B. and S.Y. contributed equally to this work. The authors would like to acknowledge Raul F. Lobo for suggestions during the course of the investigation. This work was supported by the University of Delaware Startup Fund. V.B.R.B. and G.S.H. would like to acknowledge C. Ni and F. Kriss of the W. M. Keck Electron Microscopy Facility at the University of Delaware for providing the electron-microscope time and help. V.B.R.B. would also like to acknowledge the US Department of Energy Basic Energy Sciences under Grant No. DE-FG02-07ER15921 and DE-FG02-99ER14998 for funding. The authors would also like to acknowledge technical support from Beamline X10c at NSLS, BNL.

Received: July 30, 2012
Published online: September 28, 2012

[1] J. K. Hurst, *Science* **2010**, *328*, 315.
[2] L. Hammarstrom, J. R. Winkler, H. B. Gray, S. Styring, *Science* **2011**, *333*, 288.
[3] G. D. Scholes, G. R. Fleming, A. Olaya-Castro, R. van Grondelle, *Nat. Chem.* **2011**, *3*, 763.
[4] S. Dahl, I. Chorkendorff, *Nat. Mater.* **2012**, *11*, 100.
[5] A. Paracchino, V. Laporte, K. Sivula, M. Gratzel, E. Thimsen, *Nat. Mater.* **2011**, *10*, 456.
[6] R. Asahi, T. Morikawa, T. Ohwaki, K. Aoki, Y. Taga, *Science* **2001**, *293*, 269.
[7] M. Gratzel, *Nature* **2001**, *414*, 338.
[8] Z. G. Zou, J. H. Ye, K. Sayama, H. Arakawa, *Nature* **2001**, *414*, 625.
[9] P. V. Kamat, *J. Phys. Chem. B* **2002**, *106*, 7729.
[10] S. U. M. Khan, M. Al-Shahry, W. B. Ingler, *Science* **2002**, *297*, 2243.
[11] M. Gratzel, *Inorg. Chem.* **2005**, *44*, 6841.
[12] K. Maeda, K. Teramura, D. L. Lu, T. Takata, N. Saito, Y. Inoue, K. Domen, *Nature* **2006**, *440*, 295.
[13] P. V. Kamat, *J. Phys. Chem. C* **2007**, *111*, 2834.
[14] A. Kudo, Y. Miseki, *Chem. Soc. Rev.* **2009**, *38*, 253.
[15] F. M. Toma, A. Sartorel, M. Iurlo, M. Carraro, P. Parisse, C. Maccato, S. Rapino, B. R. Gonzalez, H. Amenitsch, T. Da Ros, L. Casalis, A. Goldoni, M. Marcaccio, G. Scorrano, G. Scoles, F. Paolucci, M. Prato, M. Bonchio, *Nat. Chem.* **2010**, *2*, 826.
[16] F. Jiao, H. Frei, *Energy Environ. Sci.* **2010**, *3*, 1018.
[17] M. W. Kanan, D. G. Nocera, *Science* **2008**, *321*, 1072.
[18] F. A. Frame, T. K. Townsend, R. L. Chamousis, E. M. Sabio, T. Dittrich, N. D. Browning, F. E. Osterloh, *J. Am. Chem. Soc.* **2011**, *133*, 7264.
[19] T. K. Townsend, E. M. Sabio, N. D. Browning, F. E. Osterloh, *Energy Environ. Sci.* **2011**, *4*, 4270.
[20] C. Wang, Z. G. Xie, K. E. deKrafft, W. L. Lin, *J. Am. Chem. Soc.* **2011**, *133*, 13445.
[21] Y. Q. Cong, H. S. Park, H. X. Dang, F. R. F. Fan, A. J. Bard, C. B. Mullins, *Chem. Mater.* **2012**, *24*, 579.
[22] D. E. Wang, R. G. Li, J. Zhu, J. Y. Shi, J. F. Han, X. Zong, C. Li, *J. Phys. Chem. C* **2012**, *116*, 5082.
[23] Y. Yamada, K. Yano, D. C. Hong, S. Fukuzumi, *Phys. Chem. Chem. Phys.* **2012**, *14*, 5753.
[24] Y. Umena, K. Kawakami, J. R. Shen, N. Kamiya, *Nature* **2011**, *473*, 55.
[25] M. Hara, C. C. Waraksa, J. T. Lean, B. A. Lewis, T. E. Mallouk, *J. Phys. Chem. A* **2000**, *104*, 5275.
[26] R. Brimblecombe, G. F. Swiegers, G. C. Dismukes, L. Spiccia, *Angew. Chem. Int. Ed.* **2008**, *47*, 7335.
[27] A. J. Esswein, M. J. McMurdo, P. N. Ross, A. T. Bell, T. D. Tilley, *J. Phys. Chem. C* **2009**, *113*, 15068.
[28] M. Risch, V. Khare, I. Zaharieva, L. Gerencser, P. Chernev, H. Dau, *J. Am. Chem. Soc.* **2009**, *131*, 6936.
[29] R. Brimblecombe, A. Koo, G. C. Dismukes, G. F. Swiegers, L. Spiccia, *J. Am. Chem. Soc.* **2010**, *132*, 2892.
[30] Y. Gorlin, T. F. Jaramillo, *J. Am. Chem. Soc.* **2010**, *132*, 13612.
[31] M. M. Najafpour, T. Ehrenberg, M. Wiechen, P. Kurz, *Angew. Chem. Int. Ed.* **2010**, *49*, 2233.
[32] D. M. Robinson, Y. B. Go, M. Greenblatt, G. C. Dismukes, *J. Am. Chem. Soc.* **2010**, *132*, 11467.
[33] Q. S. Yin, J. M. Tan, C. Besson, Y. V. Geletii, D. G. Musaev, A. E. Kuznetsov, Z. Luo, K. I. Hardcastle, C. L. Hill, *Science* **2010**, *328*, 342.
[34] Y. V. Geletii, Z. Q. Huang, Y. Hou, D. G. Musaev, T. Q. Lian, C. L. Hill, *J. Am. Chem. Soc.* **2009**, *131*, 7522.
[35] S. W. Kohl, L. Weiner, L. Schwartsburd, L. Konstantinovski, L. J. W. Shimon, Y. Ben-David, M. A. Iron, D. Milstein, *Science* **2009**, *324*, 74.
[36] D. A. Lutterman, Y. Surendranath, D. G. Nocera, *J. Am. Chem. Soc.* **2009**, *131*, 3838.
[37] X. Sala, I. Romero, M. Rodriguez, L. Escriche, A. Llobet, *Angew. Chem. Int. Ed.* **2009**, *48*, 2842.
[38] H. Dau, C. Limberg, T. Reier, M. Risch, S. Roggan, P. Strasser, *ChemCatChem* **2010**, *2*, 724.
[39] D. K. Zhong, D. R. Gamelin, *J. Am. Chem. Soc.* **2010**, *132*, 4202.
[40] F. Jiao, H. Frei, *Angew. Chem. Int. Ed.* **2009**, *48*, 1841.
[41] F. Jiao, H. Frei, *Chem. Commun.* **2010**, *46*, 2920.
[42] V. B. R. Boppana, F. Jiao, *Chem. Commun.* **2011**, *47*, 8973.
[43] M. M. Thackeray, *Prog. Solid State Chem.* **1997**, *25*, 1.
[44] A. Ogata, S. Komaba, R. Baddour-Hadjean, J. P. Pereira-Ramos, N. Kumagai, *Electrochim. Acta* **2008**, *53*, 3084.
[45] X. Wang, Y. D. Li, *Chem. Eur. J.* **2003**, *9*, 300.
[46] S. H. Kim, S. J. Kim, S. M. Oh, *Chem. Mater.* **1999**, *11*, 557.
[47] O. Prieto, M. Del Arco, V. Rives, *J. Mater. Sci.* **2003**, *38*, 2815.
[48] A. C. Gaillot, V. A. Drits, A. Manceau, B. Lanson, *Microporous Mesoporous Mater.* **2007**, *98*, 267.